Rebinding of IgE Fabs at Haptenated Planar Membranes: Measurement by Total Internal Reflection with Fluorescence Photobleaching Recovery†

B. Christoffer Lagerholm,‡ Tammy E. Starr, Zoya N. Volovyk, and Nancy L. Thompson*

Department of Chemistry, Campus Box 3290, University of North Carolina at Chapel Hill, Chapel Hill, North Carolina 27599-3290

Received July 28, 1999; Revised Manuscript Received November 24, 1999

ABSTRACT: In previous work, a general analytical theory for ligand rebinding at cell surfaces was developed for a reversible bimolecular reaction between ligands in solution and receptors on a membrane surface [Lagerholm, B. C., and Thompson, N. L. (1998) *Biophys. J. 74*, 1215−1228]. This theory can be used to predict theoretical forms for data obtained by using total internal reflection with fluorescence photobleaching recovery (TIR-FPR) [Thompson, N. L., Burghardt, T. P., and Axelrod, D. (1981) *Biophys. J. 33*, 435−454]. Thus, one method by which the rebinding theory can be tested is to use TIR-FPR. In the work described herein, the reversible kinetics of mouse monoclonal anti-dinitrophenyl (DNP) IgE Fabs at substrate-supported planar membranes composed of 25 mol % DNP-conjugated phosphatidylethanolamine and 75 mol % dipalmitoylphosphatidylcholine have been examined by using TIR-FPR. Data were obtained as a function of the Fab solution concentration. Higher Fab concentrations reduce rebinding (and increase the fluorescence recovery rate) because different Fab molecules compete for the same surface-binding sites. Data were also obtained for solutions containing different volume fractions of glycerol. In these measurements, higher glycerol concentrations increase rebinding (and decrease the fluorescence recovery rate) because the solution viscosity is increased and the Fab diffusion coefficient in solution is decreased. The TIR-FPR data were quantitatively compared with theoretical predictions which follow from the general theory for rebinding at the membrane surface. The data were consistent with the theoretical predictions and, therefore, provide experimental verification of the previously developed theory.

Numerous biochemical processes are mediated by interactions between soluble ligands and cell-surface receptors. A body of previous work has theoretically addressed the thermodynamic and kinetic properties of interactions occurring between macromolecules in three-dimensional solution and sites on a planar or spherical surface (*1*−*16*). This work suggests that a phenomenon of particular importance is the process in which reversibly bound ligands dissociate from receptors, diffuse for a time in the nearby solution, and then rebind to the same or a nearby receptor on the cell surface.

We have recently presented a rigorous theoretical treatment of the rebinding process (*17*). Analytical solutions for the spatial and temporal dependence of the probabilities of finding the molecule on the surface or in solution, given initial placement at the origin, were derived. These general solutions were used to find a simple expression for the probability that a molecule rebinds to the surface at a given position and time, after initial release (not placement) at the origin. The probability expressions quantitatively predict the manner in which total internal reflection−fluorescence photobleaching recovery (TIR-FPR)[1] data should depend on the intrinsic kinetic association and dissociation rates as well as parameters such as the diffusion coefficient of ligands in solution and the density of surface binding sites (*18*). Therefore, one manner in which the general rebinding theory may be tested is by using TIR-FPR.

In the work described herein, the reversible kinetics of mouse monoclonal anti-dinitrophenyl (DNP) IgE Fabs at substrate-supported planar membranes composed of 25 mol % DNP-conjugated phosphatidylethanolamine and 75 mol % dipalmitoylphosphatidylcholine have been examined with TIR-FPR. Data obtained as a function of the IgE Fab solution concentration and as a function of the solution viscosity both qualitatively and quantitatively verify the previously developed theory for ligand rebinding at planar surfaces.

THEORETICAL BACKGROUND

The rebinding of dissociated ligands at planar membrane surfaces has been considered previously (Figure 1; *17*, *18*).

† This work was supported by National Institutes of Health Grant GM-37145 and by National Science Foundation Grant MCB-9728116.

* To whom correspondence should be addressed. Phone: (919) 962-0328. Fax: (919) 962-2388. E-mail: nlt@unc.edu.

‡ Present address: Center for Light Microscope Imaging and Biotechnology, Carnegie Mellon University, 4400 Fifth Avenue, Pittsburgh, PA 15213.

[1] Abbreviations: DMEM/F12, Dulbecco's Modified Eagle's Medium/Ham's F12; DNP-G, *N*-2,4-dinitrophenylglycine; DNP-HSA, dinitrophenyl-conjugated human serum albumin; DNP-cap-DPPE, 1,2-dipalmitoyl-*sn*-glycero-3-phosphoethanolamine-*N*-[6-[(2,4,6-dinitrophenyl)amino]caproyl]; DPPC, 1,2-dipalmitoyl-*sn*-glycero-3-phosphocholine; F-, fluorescein isothiocyanate conjugate; FPPR, fluorescence pattern photobleaching recovery; NBD-DPPE, 1,2,-dipalmitoyl-*sn*-glycero-3-phosphoethanolamine-*N*-(7-nitro-2-1,3-benzoxadiazol-4-yl); PBS, phosphate-buffered saline; TIR-FPR, total internal reflection with fluorescence photobleaching recovery; TIRFM, total internal reflection fluorescence microscopy.

10.1021/bi9917434 CCC: $19.00
Published on Web 01/28/2000

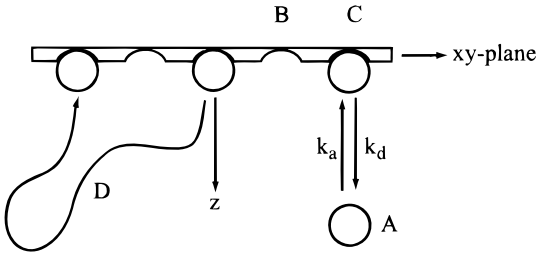

FIGURE 1: Schematic of rebinding phenomenon. Ligands in solution, A, are in equilibrium with free binding sites, B, and occupied surface binding sites, C. The association and dissociation rate constants are k_a and k_d, respectively. Ligands dissociate from the surface, explore the solution with diffusion coefficient, D, and rebind to the surface at later times and at different positions. The probability of finding a tagged molecule on the surface at a given time and position, given that the molecule was placed at the origin at time zero, is $P_C(r,t)$ (eq 7). The probability of finding a tagged molecule on the surface at a given time and position, given that the molecule dissociated at time zero, is $W(r,t)$ (eqs 3 and 4).

In these works, ligands in solution, A, reversibly associate with sites on a surface, B, to form complexes, C:

$$A + B \underset{k_d}{\overset{k_a}{\rightleftharpoons}} C \tag{1}$$

In eq 1, k_a and k_d are the kinetic association and dissociation rates, respectively. The equilibrium dissociation constant is $K_d = k_d/k_a$, and the total density of binding sites is $N = B + C$. At equilibrium,

$$C = \frac{AN}{K_d + A} \tag{2}$$

It is assumed that ligands in solution diffuse with coefficient D and that both free and occupied surface binding sites do not diffuse appreciably within the membrane plane.

The probability that a ligand which dissociates at time zero from the origin rebinds to the surface between time t and $t + dt$, position x and $x + dx$, and position y and $y + dy$, is

$$W(r,t)d^2r\,dt = \frac{1}{4\pi Dt}\exp\left(-\frac{r^2}{4Dt}\right)Y(t)d^2r\,dt \tag{3}$$

where $\boldsymbol{r} = (x,y)$. The integral of $W(r,t)$ over the (infinite) membrane plane gives the probability that the molecule rebinds somewhere on the surface between time t and $t + dt$, given release at time zero. This probability is

$$Y(t)\,dt = \left(\frac{b}{\sqrt{\pi k_d t}} - b^2 w[ib\sqrt{k_d t}]\right)k_d dt \tag{4}$$

where $w[i\zeta] = \exp(\zeta^2)\,\mathrm{erfc}(\zeta)$. The "rebinding parameter", b, is

$$b = \sqrt{\frac{k_d}{k_t}} \tag{5}$$

where

$$k_t = \frac{D}{N^2}(K_d + A)^2 \tag{6}$$

The transport rate, k_t, is the rate for diffusion in solution through a distance equal to the ratio of the ligand surface density, C, and the solution concentration, A (eq 2). Typical values of k_t are shown in Figure 2. If $k_d \ll k_t$, then $b \ll 1$, and $Y(t)$ is low but finite at all times. If $k_d \gg k_t$, then $b \gg 1$, and $Y(t)$ is high at short times and very low at long times. The integral of $Y(t)$ is unity; a previously dissociated molecule always rebinds to a planar surface of infinite extent. However, for low b values, rebinding occurs on the average at much later times after dissociation; for high b values, rebinding occurs on the average at much shorter times.

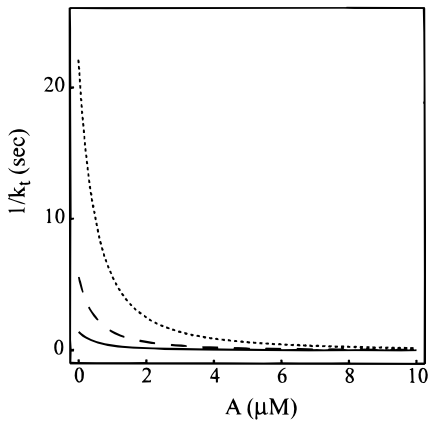

FIGURE 2: Typical values of the transport rate k_t. The inverse transport rate, $1/k_t$, is shown as a function of the ligand solution concentration, A, for $K_d = 1\ \mu$M and $D = 5 \times 10^{-7}$ cm^2/s. The values of N are (line) 5000 molecules/μm^2, (dash) 10 000 molecules/μm^2, and (dot) 20 000 molecules/μm^2, respectively.

The analytical expressions for $W(r,t)$ and $Y(t)$ (eqs 3 and 4) are what we seek to experimentally verify. As described previously (*17*), these expressions can be used to find the probabilities of finding a molecule on the surface, $P_C(r,t)$, or in solution, $P_A(r,z,t)$, given initial placement at the origin at time zero. These functions are

$$P_C(r,t) = \frac{1}{2\pi}\int_0^\infty J_0(qr)\exp(-Dq^2t)\sum_{i=1}^{3} C_i(q)w[-i\sqrt{\alpha_i t}]q\,dq \tag{7}$$

$$P_A(r,z,t) = \frac{1}{2\pi}\frac{k_d}{\sqrt{D}}\int_0^\infty J_0(qr)\exp\left[-Dq^2t - \frac{z^2}{4Dt}\right]\times \sum_{i=1}^{3} A_i(q)w\left[i\left(\frac{z}{\sqrt{4Dt}} - \sqrt{\alpha_i t}\right)\right]q\,dq \tag{8}$$

where $J_0(qr)$ is the zeroeth order Bessel function. The rates, α_i, are given by the roots of the cubic equation

$$\alpha_i^{3/2} + b\sqrt{k_d}\,\alpha_i + (k_d - Dq^2)\,\alpha_i^{1/2} - Dq^2 b\sqrt{k_d} = 0 \tag{9}$$

and the amplitudes of the monotonically decaying w-functions are

$$C_i(q);A_i(q) = \frac{\sqrt{\alpha_i}}{(\sqrt{\alpha_i} - \sqrt{\alpha_j})(\sqrt{\alpha_i} - \sqrt{\alpha_k})}(\sqrt{\alpha_i} + b\sqrt{k_d};1) \tag{10}$$

where $i \neq j \neq k$.

The functions $W(r,t)$ and $P_C(r,t)$ are not equivalent. The former gives the probability of finding a molecule on the surface given that the molecule dissociated from the origin

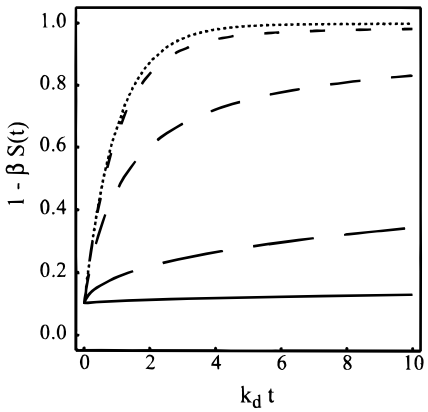

FIGURE 3: Theoretical shape of the fluorescence recovery curves. The theoretical shape of the normalized fluorescence recovery curve $F(t)/F(-)$ is shown as a function of time. The function $F(t)/F(-)$ was calculated from eqs 11, 12, and 15 with the rebinding parameter b equal to (line) 100, (long dash) 10, (dash) 1, (short dash) 0.1, and (dot) 0.01. The bleached fraction, β, is 0.90.

at time zero. The latter gives the probability of finding a molecule on the surface given that the molecule was placed on the surface at the origin at time zero. $P_C(r,t)$ is the sum of the probabilities that the molecule, once placed on the surface, has not dissociated; has dissociated, rebound, and remained on the surface; has dissociated, rebound, dissociated, rebound, and remained on the surface; and so forth.

The integral of $P_C(r,t)$ over the infinite membrane plane is

$$S(t) = \frac{u_2 w[-iu_1\sqrt{k_d t}] - u_1 w[-iu_2\sqrt{k_d t}]}{u_2 - u_1} \qquad (11)$$

where

$$u_{1,2} = -\frac{b}{2} \pm \sqrt{\frac{b^2}{4} - 1} \qquad (12)$$

The function $S(t)$ is related to $Y(t)$ in a manner analogous to the one in which $P_C(r,t)$ is related to $W(r,t)$. When $b \ll 1$,

$$\lim_{b\to 0} S(t) = \exp(-k_d t) \qquad (13)$$

When $b \gg 1$,

$$\lim_{b\to \infty} S(t) = w[i\sqrt{k_t t}] \qquad (14)$$

In the limit of a large bleached and observed area, the recovery curve measured by TIR-FPR (i.e., the fluorescence arising from surface-bound molecules as a function of time) is (*18*)

$$\frac{F(t)}{F(-)} = 1 - \beta S(t) \qquad (15)$$

where $F(-)$ is the prebleach fluorescence, and β is the fraction of the fluorescence which is bleached. This function, which is plotted in Figure 3, depends only on the rates k_t and k_d. When $k_d \ll k_t$, recovery is limited only by the intrinsic dissociation rate. This limit is the one in which $b \ll 1$ and rebinding is not prominent (eq 13). When $k_d \gg k_t$, recovery is limited by the rate of solution diffusion. This limit is the one in which $b \gg 1$ and rebinding is prominent (eq 14). The rate k_t may be experimentally altered by changing the ligand solution concentration, A, or the ligand diffusion coefficient, D, by varying the solution viscosity. Quantitative agreement of measured TIR-FPR recovery curves with eqs 5, 6, 11, 12, and 15 experimentally verifies eqs 3 and 4.

MATERIALS AND METHODS

Intact IgE. Anti-dinitrophenyl (DNP) IgEs were obtained from the hybridoma TIB142 (American Type Culture Collection, Rockville, MD) (*19*). Hybridomas were maintained in culture in DMEM/F12 medium supplemented with 1 mM sodium pyruvate, 2 mM L-glutamine, 100 IU of penicillin G, 100 μg/mL streptomycin, and 5% heat-inactivated (30 min, 56 °C) fetal calf serum. Monoclonal anti-DNP IgE antibodies were purified from TIB142 supernatants by affinity chromatography with DNP-conjugated human serum albumin (DNP-HSA) (*20*). The IgE was eluted with 10 mM dinitrophenylglycine (DNP-G) in phosphate-buffered saline (PBS; 50 mM sodium phosphate, 0.15 M sodium chloride, 0.01% sodium azide, pH 7.4). Residual DNP-G was removed by extensive dialysis against PBS. IgE concentrations were estimated spectrophotometrically by assuming that ϵ(IgE, 280 nm) = 298 000 M^{-1} cm^{-1}.

IgE Fabs. Anti-DNP IgE Fabs were produced from intact IgE by digestion with papain (*20*, *21*). Intact IgE (1−3 mg/mL) in 100 mM sodium acetate (pH 5.5) with 50 μM cysteine and 10 mM EDTA was treated with preactivated (30 min, 37 °C) papain (Worthington Biochemical Corporation, Freehold, NJ) at a ratio of 10 μg of papain/mg of IgE for 23 h at 37 °C. The reaction was quenched by adding 50 mM iodoacetamide for 1 h at 0 °C followed by dialysis into PBS. IgE Fabs were purified by DNP-HSA affinity chromatography (see above) followed by gel exclusion chromatography (Sephadex G150, 1.5 cm × 55 cm, 0.2 mL/min). Fractions containing no detectable amount of undigested, intact IgE (as monitored by SDS−PAGE with silver staining) were pooled for future use. Residual DNP-G was removed by passing the IgE Fabs in 0.01 M sodium phosphate, 0.1 M sodium chloride, 0.01% sodium azide (pH 5.7) through a Dowex 1X8-200 ion-exchange column (*22*). IgE Fab concentrations were estimated from the optical densities at 280 nm and an assumed molar absorptivity of ϵ(IgE Fab, 280 nm) = 70 000 M^{-1} cm^{-1}.

Fluorescence Labeling. IgEs were fluorescently labeled (F-) as previously described (*23*). Fabs at 0.2−0.8 mg/mL were dialyzed into 0.1 M $NaHCO_3$ (pH 9.2) and treated with a 10-fold molar excess of fluorescein isothiocyanate (Molecular Probes, Inc., Eugene, OR). Unreacted fluorescein was removed by gel exclusion chromatography with Sephadex G50 in PBS followed by dialysis against PBS. The concentration of F-(IgE Fab) and the molar ratio of fluorescein to IgE Fab were determined spectrophotometrically using the molar absorptivity of IgE Fab at 280 nm (see above) and the following molar absorptivities for fluorescein: ϵ(fluorescein, 494 nm) = 75 000 M^{-1} cm^{-1} and ϵ(fluorescein, 280 nm) = 18 750 M^{-1} cm^{-1}. The molar ratio of fluorescein to IgE Fab ranged from 0.25 to 0.8.

IgE Fab Solutions for Planar Membranes. F-(IgE Fab) were dialyzed into either PBS, PBS/glycerol (75/25, vol/vol), or PBS/glycerol (65/35, vol/vol). The viscosities of these

Table 1: Specificity of F-(IgE Fab) Binding to Planar Membranes[a]

planar membrane composition	DNP-G (μM)	glycerol (volume fraction)		
		0	25	35
DNP-cap-DPPE/DPPC	0	1	1	1
DPPC	0	0.045 ± 0.003	0.022 ± 0.001	0.0087 ± 0.0004
DNP-cap-DPPE/DPPC	100	0.054 ± 0.001	0.061 ± 0.001	0.069 ± 0.001

[a] The relative surface-associated fluorescence intensities of F-(IgE Fab) were measured by using TIRFM. The solution concentrations of F-(IgE Fab) and DNP-G were 1 and 100 μM, respectively. Values are the means of nine spatially independent measurements on each of 1−4 independently prepared samples for each sample type. For each solvent condition, each mean value was normalized by the value for F-(IgE Fab) on DNP-cap-DPPE/DPPC membranes in the absence of DNP-G. The averages of the normalized means were determined for each sample type. Uncertainties are standard deviations of the means.

solutions were confirmed with a Cannon-Fenske Routine Type Viscometer (Cannon Instrument Co., State College, PA). F-(IgE Fab) solutions were clarified by air ultracentrifugation (130000*g*, 30 min, 25 °C) immediately before use.

Phospholipid Vesicles. Small unilamellar vesicles were prepared from 1,2-dipalmitoyl-*sn*-glycero-3-phosphocholine (DPPC), 1,2-dipalmitoyl-*sn*-glycero-3-phosphoethanolamine-*N*-[6-[(2,4,6-dinitrophenyl)amino]caproyl] (DNP-cap-DPPE), and 1,2-dipalmitoyl-*sn*-glycero-3-phosphoethanolamine-*N*-(7-nitro-2-1,3-benzoxadiazol-4-yl) (NBD-DPPE) (Avanti Polar Lipids, Birmingham, AL). Vesicles were prepared by tip sonication of 2 mM suspensions of DPPC, DNP-cap-DPPE:DPPC (25/75, mol/mol), or DNP-cap-DPPE:DPPC:NBD-DPPE (24/74/2, mol/mol/mol) in deionized water as previously described (24).

Planar Membranes. Supported planar membranes were deposited on fused silica substrates (*19*, *24*). Substrates (1″ × 1″ × 1 mm) (Quartz Scientific, Fairport Harbor, OH) were cleaned by boiling in detergent (Lot 08778, ICN, Aurora, OH), bath sonicating, and rinsing extensively with deionized water. Immediately before use, substrates were cleaned in an argon ion plasma cleaner (20 min, 25 °C) (PDC-3XG, Harrick Scientific, Ossining, NY). Supported planar membranes were constructed by depositing vesicles onto the fused silica surfaces (30 min, 25 °C) followed by rinsing with 3 mL of PBS or PBS/glycerol. Planar membranes were treated with 250 μL of various concentrations of F-(IgE Fab) and DNP-G in PBS or PBS/glycerol.

Fluorescence Microscopy. Steady-state TIRFM, TIR-FPR, and fluorescence pattern photobleaching recovery (FPPR) measurements were carried out on an instrument consisting of an argon ion laser (Innova 90-3; Coherent, Palo Alto, CA), an inverted microscope (IM-35; Zeiss, Eastern Microscope Co., Raleigh, NC), and a single-photon counting photomultiplier (31034A; RCA, Lancaster, PA). The experimental parameters for steady-state TIRFM (*25*−*27*), TIR-FPR (*24*, *28*, *29*), and FPPR (*30*−*32*) have been described previously. When incident on the fused silica/aqueous interface, the laser beam was s-polarized and generated an evanescent field polarized parallel to the interface. Fluorescence recovery curves were monitored for 50−200 s after photobleaching; longer times were used for slower recoveries. Data were curvefit to theoretical forms by using Mathematica (Wolfram Research Inc., Champaign, IL) software packages.

RESULTS

Planar Membranes. Solidlike phospholipid membranes were deposited on planar fused silica substrates by allowing probe sonicated phospholipid vesicles to adsorb to and fuse at the surfaces, as previously described (*19*, *24*, *27*, *28*, *33*). Membranes composed of DNP-cap-DPPE/DPPC/NBD-DPPE (24/74/2, mol/mol/mol) or DPPC/NBD-DPPE (98/2, mol/mol) appeared uniformly fluorescent within optical resolution. The translational mobility of the fluorescent lipids was monitored by using FPPR as previously described (*30*−*32*). These measurements indicated that ≤10% of the fluorescent lipids were translationally mobile with an apparent diffusion coefficient of $\leq 5 \times 10^{-10}$ cm^2/s, for both PBS and PBS/glycerol solutions.

Specificity of IgE Fab Binding to Planar Membranes. The steady-state fluorescence arising from F-(IgE Fab) bound or adjacent to supported planar membranes was measured with TIRFM as previously described (*21*, *24*−*27*, *34*). This surface-associated fluorescence was much higher in the presence of DNP-cap-DPPE and the absence of DNP-G (Table 1). The nonnegligible fluorescence on the negative controls can be attributed to the combination of fluorescence arising from F-(IgE Fab) in solution but close enough to the surface to be within the finite depth of the evanescent field and from F-(IgE Fab) nonspecifically bound to the planar membrane surfaces.

Equilibrium Dissociation Constants for F-(IgE Fab) Binding to Planar Membranes. Equilibrium dissociation constants for F-(IgE Fab) binding to DNP-cap-DPPE/DPPC planar membranes were determined by using steady-state TIRFM (*21*, *24*−*27*, *34*). The evanescently excited fluorescence of F-(IgE Fab) on DNP-cap-DPPE membranes was measured as a function of the F-(IgE Fab) solution concentration. Control measurements were carried out in which the membranes were composed only of DPPC and in which the solution contained 100 μM DNP-G. The fluorescence was higher and began to saturate with increasing concentrations of F-(IgE Fab) on membranes containing DNP-cap-DPPE and in the absence of DNP-G. The fluorescence was lower and linear with the F-(IgE Fab) solution concentration for DPPC membranes and in the presence of 100 μM DNP-G. Similar results were obtained for measurements carried out in PBS, PBS/glycerol (75/25, v/v), or PBS/glycerol (65/35, v/v).

To measure the equilibrium dissociation constants K_d, the data for a given set of three control samples of a given type were fit to a line. The theoretical values of this line were subtracted from the data for a matched set of six positive samples, and the difference data were fit to the theoretical form for a reversible bimolecular reaction (eq 2). In this analysis, the experimentally determined parameters were the F-(IgE Fab) solution concentrations and the (corrected)

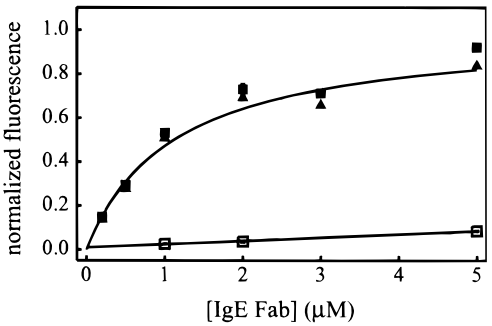

FIGURE 4: Representative TIRFM equilibrium binding curve for F-(IgE Fab) on planar membranes. The evanescently excited fluorescence on DNP-cap-DPPE/DPPC planar membranes in the (■) absence and (□) presence of 100 μM DNP-G is plotted as a function of the F-(IgE Fab) solution concentration. The control (□) data were fit to a line. The theoretical values of this line for different F-(IgE Fab) concentrations were subtracted from the positive data and are shown as difference data (▲). The difference data were fit to the theoretical form for a simple reversible bimolecular reaction (eq 2). The positive data are compared to the sum of this best fit and the best fit of the control data to a line. The fluorescence intensities have been normalized so that the theoretical value of the difference data at infinite antibody solution concentration is unity. Each point is the average of nine spatially independent measurements for the given sample. The standard deviations of the means associated with these averages are smaller than the point size. For this curve, the measurements were obtained in PBS without glycerol.

Table 2: Equilibrium and Kinetic Dissociation Constants for F-(IgE Fab) on DNP-cap-DPPE/DPPC Planar Membranes[a]

glycerol (volume fraction)	sets of data	K_d (μM)	k_{avg}^{∞} (s^{-1})
0	5	1.11 ± 0.03	0.39 ± 0.01
25	3	1.30 ± 0.17	0.37 ± 0.01
35	2	0.76 ± 0.06	0.34 ± 0.02
0, 25, 35	10	1.10 ± 0.03	0.37 ± 0.01

[a] Equilibrium dissociation constants, K_d, were measured for F-(IgE Fab) on DNP-cap-DPPE/DPPC membranes in PBS, PBS/glycerol (75/25, v/v), and PBS/glycerol (65/35, v/v). Each value is the average of two to five independent determinations in which six positive samples were matched with three of one of the two types of control samples (Figure 4). TIR-FPR recovery curves were fit to eq 22 (Figure 6, panels c and d). Average values of k_1, k_2, and f were determined from 11 to 25 recovery curves obtained from two to four independently prepared samples, for each sample type. Values of k_{avg} were calculated from k_1, k_2, and f (eq 23) and were fit to eq 24 (Figure 7) to determine the reaction-limited value, denoted by k_{avg}^{∞}. Uncertainties are standard deviations of the means.

surface fluorescence intensities. The free parameters were the equilibrium dissociation constant, K_d, and the extrapolated fluorescence intensity at infinite F-(IgE Fab) solution concentration. A representative equilibrium binding curve and its best fit to the theoretical form are shown in Figure 4. The best-fit values of the dissociation constants, K_d, for PBS, PBS/glycerol (75/25, v/v), and PBS/glycerol (65/35, v/v) are shown in Table 2. The small decrease in K_d at high glycerol concentration is consistent with current theories addressing the effect of cosolvents on thermodynamic activities (*35*).

Physical and Optical Properties of Glycerol Solutions. The known viscosities of aqueous solutions of glycerol (*36*) were confirmed by using a Cannon-Fenske Routine Type Viscometer (Table 3). This table also shows the known refractive indices of the solutions (*36*). The critical angle, θ_c, and the depth of the evanescent field, d, are given by

Table 3: Properties of Aqueous Glycerol Solutions[a]

	volume fraction of glycerol (υ)		
	0	25	35
viscosity (theor) (g/cm s) × 10^2	1.002	2.404	3.714
viscosity (expt) (g/cm s) × 10^2	0.95 ± 0.01	2.29 ± 0.03	3.68 ± 0.02
refractive index $n_2(\upsilon)$	1.334	1.370	1.385
critical angle θ_c (deg)	65.4	69.0	70.7
evanescent depth d (Å)	700	847	945
$I(\upsilon)/I(0)$ (theor)	1	1.36	1.59
$I(\upsilon)/I(0)$ (expt)	1	1.49 ± 0.03	1.86 ± 0.03

[a] Theoretical values for the viscosities and refractive indices are from published tables for 20 °C (*36*). Critical angles, evanescent wave depths, and interfacial intensities were calculated from eqs 16−18. Viscosities were measured by using a Cannon-Fenske Routine Type viscometer. Experimental values of $I(\upsilon)/I(0)$ were obtained from the evanescently excited fluorescence intensities of planar membranes containing the fluorescent lipid NBD-DPPE. Uncertainties are standard deviations of the means.

$$\theta_c = \sin^{-1}\frac{n_2(\upsilon)}{n_1} \tag{16}$$

$$d(\upsilon) = \frac{\lambda}{4\pi\sqrt{n_1^2 \sin^2\theta - n_2^2(\upsilon)}} \tag{17}$$

where $\lambda = 488.0$ nm is the vacuum wavelength, $n_1 = 1.467$ is the refractive index of the substrate, $\theta \approx 80°$ is the incidence angle, $n_2(\upsilon)$ is the refractive index of the aqueous solution, and υ denotes the volume fraction of glycerol (*37*). According to eqs 16 and 17, the critical angle, θ_c, is expected to increase by a factor of 1.08, and the depth $d(\upsilon)$ is expected to increase by a factor of 1.35 for PBS/glycerol (65/35) relative to PBS (Table 3). For the s-polarized incident laser beam used in this work, the evanescent field is polarized parallel to the interface. The evanescent intensity at the interface, for PBS/glycerol relative to that for PBS is (*37*)

$$\frac{I(\upsilon)}{I(0)} = \frac{n_1^2 - n_2^2(0)}{n_1^2 - n_2^2(\upsilon)} \tag{18}$$

Equation 18 predicts the relative fluorescence of substrate-supported planar membranes containing fluorescent lipids, and was verified experimentally (Table 3).

Surface Dissociation Kinetics. The kinetics of F-(IgE Fab) at DNP-cap-DPPE/DPPC planar membranes were examined by using TIR-FPR (*20*, *24*, *27*, *29*, *33*, *34*). Recovery curves were obtained for a range of F-(IgE Fab) concentrations covering the binding isotherms (Figure 4) and for volume fractions of glycerol equal to 0, 25, and 35. Control measurements indicated that the recovery curves did not change for different bleaching durations or intensities or for different monitoring intensities. Representative recovery curves are shown in Figure 5. The rate of recovery was significantly slowed by lowering the F-(IgE Fab) solution concentration or by increasing the volume fraction of glycerol.

The fluorescence recovery curves were first fit to the theoretical form having the shape of a single exponential, i.e.,

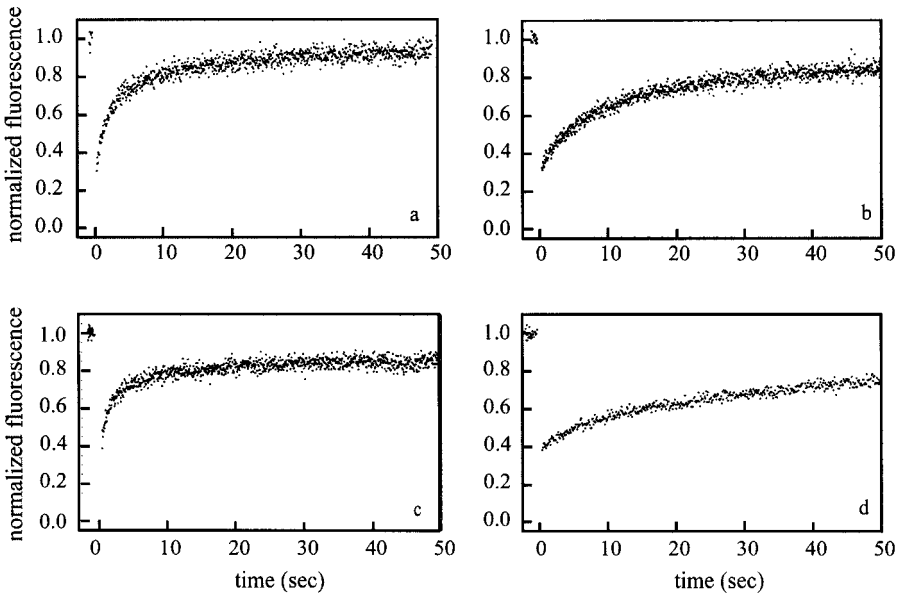

FIGURE 5: Representative TIR-FPR recovery curves for F-(IgE Fab) on DNP-cap-DPPE/DPPC planar membranes. These plots show typical fluorescence recovery curves for F-(IgE Fab) on DNP-cap-DPPE/DPPC planar membranes. The F-(IgE Fab) solution concentrations were (a, c) 5 μM and (b, d) 0.5 μM. The solvent was (a, b) PBS or (c, d) PBS/glycerol (65/35, v/v).

$$\frac{F(t)}{F(-)} = 1 - \beta\{1 - \mu[1 - \exp(-k_0 t)]\} \qquad (19)$$

where $F(-)$ is the prebleach fluorescence, $F(t)$ is the fluorescence at time t after the bleaching pulse, and k_0 is the characteristic rate. The fraction of the fluorescence which is bleached, β, is

$$\beta = \frac{F(-) - F(0)}{F(-)} \qquad (20)$$

and the fraction of the bleached fluorescence which recovers, μ, is

$$\mu = \frac{F(\infty) - F(0)}{F(-) - F(0)} \qquad (21)$$

The fluorescence recovery curves were not well fit by the single-exponential shape in eq 19 (Figure 6, panels a and b).

Because the TIR-FPR data were not well described by a single exponential, they were also fit to the theoretical form for the sum of two exponentials, i.e.,

$$\frac{F(t)}{F(-)} = 1 - \beta\{1 - \mu[1 - f\exp(-k_1 t) - (1 - f)\exp(-k_2 t)]\} \qquad (22)$$

where $k_1 > k_2$ are the two characteristic rates and f is the fraction of the fluorescence recovery associated with the faster rate. The values of the F-statistics (of the χ^2 goodness-of-fit parameter) for comparing the fits to eq 19 and eq 22 were calculated as previously described (*30*). A statistically better fit yields a value of $F > 3$. For the complete data set, the values of F were well above the critical value of three. For the highest F-(IgE Fab) solution concentrations, the average values of F were 190 ± 10 (0% glycerol), 130 ± 10 (25% glycerol), and 170 ± 20 (35% glycerol). For the lowest F-(IgE Fab) solution concentrations, the average values of F were 200 ± 30 (0% glycerol), 230 ± 20 (25% glycerol), and 80 ± 20 (35% glycerol). This analysis indicates that the TIR-FPR recovery curves were better fit by eq 22 than eq 19.

The average dissociation rate was calculated as

$$k_{avg} = f k_1 + (1-f)k_2 \qquad (23)$$

Representative fits to eq 22 are shown in Figure 6, panels c and d. For a given volume fraction of glycerol, the parameters k_1, k_2, f, and k_{avg} increased with the IgE Fab solution concentration (A) to approximately constant values. These data were fit to

$$\xi(A) = \frac{A\xi^{\infty}}{c + A} \qquad (24)$$

where $\xi = k_1$, k_2, f, or k_{avg} and ξ^{∞} and c were free parameters. Representative data and their best fit to eq 24 are shown in Figure 7. The values of $k_1^{\infty} = 0.59 \pm 0.03$ s^{-1}, $k_2^{\infty} = 0.08 \pm 0.01$ s^{-1}, $f^{\infty} = 0.55 \pm 0.01$, and $k_{avg}^{\infty} = 0.37 \pm 0.01$ s^{-1} (Table 2) are taken as the reaction-limited values. The bleach depths, β (0.3−0.9), and the fractional recoveries, μ (0.87 ± 0.05), were not correlated with any other experimental parameters and were equivalent within experimental certainty for different sample types.

Control measurements were carried out in which TIR-FPR recovery curves were obtained for two different sizes of the bleached and observed area. In these measurements, the semiminor and semimajor radii of the elliptically shaped evanescent illumination were either ≈15 and ≈40 μm or ≈35 and ≈50 μm. For both 5 μM F-(IgE Fab) in PBS and 0.2 μM F-(IgE Fab) in PBS/glycerol (65/35, v/v), the best-fit parameters k_1, k_2, f, and μ did not change with the increase in the size of the bleached and observed area, within experimental uncertainty.

VERIFICATION OF THE REBINDING THEORY

For a simple, reversible bimolecular reaction between monovalent proteins in solution and monovalent membrane

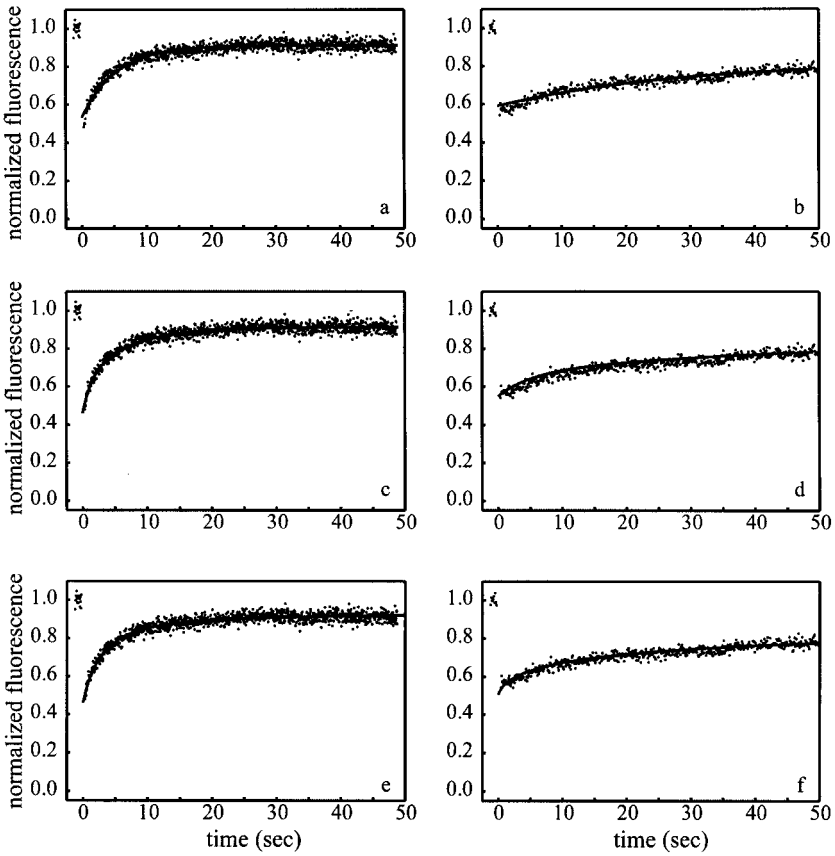

FIGURE 6: Representative best fits of TIR-FPR recovery curves to theoretical forms. These plots show two typical fluorescence recovery curves and their best fits to eqs 19, 22, and 25. The data are for (a,c,e) 5 μM F-(IgE Fab) in PBS and (b, d, f) 0.2 μM F-(IgE Fab) in PBS/glycerol (65/35, v/v). The lines show the best fits to (a, b) a single exponential (eq 19), (c, d) the sum of two exponentials (eq 22), and (e, f) the sum of two *w*-functions with $k_d = 0.37$ s^{-1} (eq 25). The best fit parameters for these two curves were (a) $k_0 = 0.19$ s^{-1}, $\mu = 0.81$; (b) $k_0 = 0.035$ s^{-1}, $\mu = 0.57$; (c) $k_1 = 0.70$ s^{-1}, $k_2 = 0.14$ s^{-1}, $f = 0.40$, $\mu = 0.84$; (d) $k_1 = 0.20$ s^{-1}, $k_2 = 0.020$ s^{-1}, $f = 0.40$, $\mu = 0.63$; (e) $b = 0.55$, $\mu = 0.84$; and (f) $b = 3.40$, $\mu = 0.69$. The ranges of the values of the reduced χ^2 goodness-of-fit statistics were 1.2−2.1 (eq 19), 1.0−1.5 (eq 22), and 1.0−2.7 (eq 25).

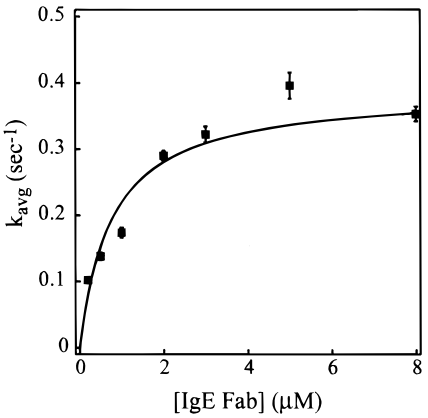

FIGURE 7: Apparent reaction-limited dissociation rate. TIR-FPR recovery curves for F-(IgE Fab) on DNP-cap-DPPE/DPPC planar membranes were fit to eq 22 (Figure 6, panels c and d). The values of k_{avg} were calculated from k_1, k_2, and f (eq 23), and were fit to eq 24. This plot shows representative data for k_{avg}(A); the solution composition was PBS without glycerol. Uncertainties are standard deviations of the means. The line shows the best fit to eq 24 with k_{avg}^{∞} and c as free parameters.

binding sites, the shapes of TIR-FPR recovery curves for a large bleached and observed area (eqs 11, 12, and 15) are predicted to depend on two characteristic rates: the intrinsic surface dissociation rate, k_d, and the rate for transport in solution through a distance equal to the ratio of the ligand surface density and ligand solution concentration, k_t (eq 6). When $k_d \ll k_t$, the fluorescence recovery curve has the shape of a single exponential with rate k_d (eq 13). In this limit, bleached molecules do not rebind to the surface after dissociation ($b \ll 1$). When $k_t \ll k_d$, the fluorescence recovery curve has a nonexponential shape with rate k_t (eq 14). In this limit, bleached molecules experience repeated dissociation and rebinding at the surface ($b \gg 1$). The purpose of the measurements described in this work is to verify that the observed fluorescence recoveries are consistent with this theoretically predicted behavior by changing the relative values of k_t and k_d.

Increasing the ligand solution concentration increases the transport rate k_t (Figure 2). Thus, the rate of fluorescence recovery is predicted to increase with A until the limit of eq 13 is reached. Higher ligand solution concentrations increase the ability of unbleached molecules to compete with bleached molecules for surface binding sites, thereby decreasing the extent of rebinding. Increasing the solvent viscosity decreases the transport rate k_t by decreasing D (eq 6). Thus, the rate of fluorescence recovery is predicted to decrease with increasing volume fractions of glycerol. Increasing the solvent viscosity decreases the ligand diffusion coefficient and inhibits the degree to which bleached molecules escape from the solvent adjacent to the bleached area before rebinding to this area.

Previous work on similar systems suggests that $N \approx 14\,000$ molecules/μm^2 (*20, 21*). In addition, $K_d \approx 1$ μM (Table 2)

and 0.2 μM < A < 8 μM (Figure 7). For PBS, D $\approx 5 \times 10^{-7}$ cm^2 s^{-1}, and eq 6 predicts that 0.1 s^{-1} < k_t < 8 s^{-1}. For PBS/glycerol (65/35, v/v), $D \approx 1.3 \times 10^{-7}$ cm^2 s^{-1} and eq 6 predicts that 0.03 s^{-1} < k_t < 2 s^{-1}. The rate of fluorescence recovery is predicted to significantly decrease for values of $b \geq 1$ (Figure 3) or $k_d \geq k_t$. Therefore, for values of k_d on the order of 1 s^{-1}, it is expected that the fluorescence recovery rate will decrease with decreasing solution concentrations and increasing volume fractions of glycerol. As shown in Figure 5, these predictions were qualitatively verified.

Equation 15 describes the effect of rebinding on TIR-FPR recovery curves for samples in which the size of the bleached and observed area is large. In theory, decreasing this area reduces the degree to which rebinding of bleached molecules to the surface slows fluorescence recovery (*18*). This effect appears mathematically in the form of a characteristic rate equal to $k_s = 4D/s^2$, where s is the semiminor axis of the elliptically shaped, bleached area. In this work, for most of the measurements, $s \approx 15$ μm and $k_s \approx 0.5$ s^{-1}. Because this rate is on the order of k_d and k_t, measurements were carried out in which TIR-FPR recovery curves were measured on matched samples for different values of s (15 and 35 μm). In these measurements, the kinetic parameters did not change within experimental uncertainty. Therefore, the effects of the size of the bleached and observed area on the rate of fluorescence recovery were assumed to be negligible compared to the effects of changing the solution concentration of F-(IgE Fab) or the solvent viscosity.

The fluorescence recovery curves are not well described by a single exponential, even for the highest solution concentrations and in the absence of glycerol (Figure 6a). A possible explanation for this result is that even at high solution concentrations, the system is not completely reaction limited; i.e., some rebinding of bleached molecules still occurs. However, nonexponential shapes have been observed for most, if not all, previous measurements in which TIR-FPR has been used to examine protein−membrane dissociation kinetics even when the systems are thought to be entirely determined by the intrinsic dissociation rate k_d (*20*, *24*, *27*, *29*, *38*). Indeed, nonexponential data are usually observed for the kinetics of protein-membrane binding monitored by most techniques (*39*−*49*).

The mechanism governing the nonexponential nature of the kinetic data for high-concentrations of F-(IgE Fab) on DNP-cap-DPPE/DPPC planar membranes is not known. The two simplest generalizations of the mechanism shown in eq 1 are one in which membrane-bound IgE Fabs are assumed to undergo an isomerization (discrete states in series) and one in which the membranes are assumed to present two types of binding sites (discrete states in parallel). The nature of rebinding at planar surfaces and the predicted shapes of TIR-FPR recovery curves for these mechanisms are known (*50*, *51*), but the formalism is complex. Therefore, we have proceeded to analyze the data with the theory for rebinding described above and in which the intrinsic dissociation rate k_d is assumed to be equal to the limit of the average rate, k_{avg}, calculated from the fit to a sum of two exponentials, as A approaches infinity. The limiting values of k_{avg}, denoted by k_{avg}^{∞}, were found by fitting data like those in Figure 7 to eq 24 and are shown in Table 2. As shown, $k_{avg}^{\infty} = 0.37$ s^{-1} and did not change with the volume fraction of glycerol.

Using the single dissociation rate k_{avg}^{∞}, we have examined the manner in which the TIR-FPR recovery curves change with respect to two experimental parameters which are expected to affect the rebinding process, the F-(IgE Fab) solution concentration and the solvent viscosity. This method of analysis emphasizes the general features of the rebinding phenomenon rather than the mechanism underlying the heterogeneity in the intrinsic dissociate rates.[2] The full set of TIR-FPR recovery curves were fit to the following modification of eq 15:

$$\frac{F(t)}{F(-)} = 1 - \beta\{1 - \mu[1 - S(t)]\} \qquad (25)$$

where $S(t)$ is given by eqs 11 and 12. The value of k_d was fixed at 0.37 s^{-1}, and the free parameters were the rebinding parameter b, the fractional bleach β, and the fractional recovery μ (which was constrained to be ≤ 1). Representative best fits are shown in Figure 6, panels e and f.

The values of b are predicted to depend on the F-(IgE Fab) solution concentration as (eqs 5 and 6) (Figure 2)

$$b^2 = \frac{\sigma}{(K_d + A)^2} \qquad (26)$$

where σ is given below in eq 27. The best-fit values of b^2 were fit to eq 26 with K_d fixed at the values shown in Table 2 and σ as a free parameter (Figure 8). The parameter σ is predicted to equal

$$\sigma = \frac{k_d N^2}{D} \propto \eta \qquad (27)$$

where η is the solvent viscosity. A plot of σ as a function of k_d/D is linear with a slope of 640 μM^2 μm^2 (Figure 8, inset). The slope implies that $N = 15\,000$ molecules/μm^2. This value is consistent with previous estimates (*20*, *21*). Therefore, the best fit values of b are consistent with the previously derived theory for ligand rebinding at planar surfaces.

SUMMARY

A large variety of biochemical processes are mediated by interactions between soluble ligands and receptors on cell membranes. A key feature of these processes is that they occur at the interface of three-dimensional solution and a two-dimensional surface. This physical feature implies that the mechanisms by which ligand−receptor interactions proceed may be complicated by the interplay between the intrinsic chemistry of the ligand−receptor interaction and transport in solution. One phenomenon that is thought to be of particular importance is the process in which reversibly

[2] One might question the effect of using the average rate, k_d^{∞}, rather than the fast rate, k_1^{∞}, or the slow rate, k_2^{∞}. An F-statistic analysis (see text) of the χ^2 values for the best fits to eq 25 indicated that the fits were much better for analyses using k_d^{∞} rather than k_2^{∞} ($F \approx 1.5 \times 10^4$) and were better for analyses using k_d^{∞} rather than k_1^{∞} ($F \approx 220$). For k_2^{∞}, the fits were too poor for further analysis. For k_1^{∞}, the best fit values of b depended on the F-(IgE Fab) solution concentration and the solvent viscosity in a manner similar to that for k_d^{∞} (Figure 8). Furthermore, the value of $N = 17\,000$ molecules/μm^2 was not significantly changed.

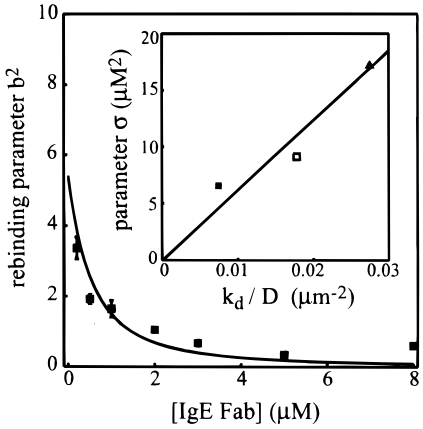

FIGURE 8: Rebinding parameter *b*. TIR-FPR recovery curves for F-(IgE Fab) on DNP-cap-DPPE/DPPC planar membranes were fit to eqs 11, 12, and 25 with $k_d = 0.37\ s^{-1}$ and with *b*, β, and $\mu \leq 1$ as free parameters. The best fit values of b^2 are shown as a function of the F-(IgE Fab) solution concentration for PBS without glycerol. Uncertainties are standard deviations of the means. The line shows the best fit of the data to eq 26 with σ as a free parameter. (Inset) The best fit values of the constants σ are proportional to the solvent viscosity, η. Data are shown for volume fractions of glycerol equal to (■) 0, (□) 25, and (▲) 35; the diffusion coefficient was assumed to equal 5.0, 2.1, and 1.3×10^{-7} cm²/s, respectively (Table 3), and $k_d = 0.37\ s^{-1}$. Linear regression gives a slope equal to 640 $\mu M^2\ \mu m^2$. The slope implies a reasonable value for the site density (see text).

bound ligands dissociate from receptors, diffuse for a time in the nearby solution, and then rebind to the same or a nearby receptor on the cell membrane (Figure 1).

In a previous work, we presented a rigorous theoretical treatment of the rebinding process for the case in which monovalent ligands reversibly bind to monovalent sites on surfaces (*17*). Analytical solutions for the probabilities of finding a tagged molecule on the surface or in the solution, given initial placement at the origin, were derived (eqs 7 and 8). These general analytical solutions were used to find more simple expressions for the probability that a molecule rebinds to the surface at a given position and time, after initial release from the origin (eqs 3 and 4).

These previously derived probability expressions imply known theoretical forms for the shapes of TIR-FPR recovery curves (*18*) (eqs 11, 12, and 15). For large bleached and observed areas, the recovery curves may be reaction limited, where they depend only on the intrinsic surface dissociation rate k_d (eq 13); diffusion limited, where they depend only on a transport rate k_t (eq 14); or partially diffusion limited, where they depend on both rates (eqs 11 and 12) (Figure 3). The rate k_t depends on the diffusion coefficient in solution, the density of surface binding sites, the equilibrium dissociation constant, and the ligand solution concentration (eq 6) (Figure 2).

In the work described here, we have tested the rebinding theory by examining TIR-FPR data for fluorescently labeled anti-DNP IgE Fabs reversibly associating with substrate-supported planar membranes composed of DNP-cap-DPPE and DPPC. The data were qualitatively consistent with the theory in that the fluorescence recovery slowed when the solution concentration of IgE Fab was reduced or when the solvent viscosity was increased[3] (Figure 5). The data were quantitatively consistent with the theory in that the measured values of the rebinding parameter *b*, which report the relative values of k_d and k_t (eq 5), changed with the IgE Fab solution concentration as theoretically predicted, and the manner in which the parameter *b* changed with the solution viscosity was consistent with the known surface site binding density (Figure 8). It is therefore reasonable to use the value of the parameter *b* (eq 5) for a given ligand−receptor system to determine the extent to which the ligand will rebind to the same or an adjacent cell-surface receptor after dissociation.

[3] In this experimental system, it is not possible to change the surface site density, *N*, in a quantitatively rigorous manner. A large fraction of the Fab binding sites presented by the DNP-cap-DPPE phospholipids are not accessible for antibody binding, and the density of accessible binding sites is not a simple function of the ratio of DNP-cap-DPPE and DPPC (*20*, *21*, *31*).

ACKNOWLEDGMENT

We thank Kevin P. Troyer for initial experimental measurements and Alena M. Lieto for assistance with IgE Fab preparations.

REFERENCES

1. Adam, G., and Delbrück, M. (1968) in *Structural Chemistry and Molecular Biology* (Rich, A., and Davison, N., Eds.) pp 198−215, W. H. Freeman, San Francisco.
2. Berg, H. C., and Purcell, E. M. (1977) *Biophys. J. 20*, 193−219.
3. DeLisi, C., and Wiegel, F. W. (1981) *Proc. Natl. Acad. Sci. U.S.A. 78*, 5569−5572.
4. Shoup, D., and Szabo, A. (1982) *Biophys. J. 40*, 33−39.
5. Berg, O., and von Hippel, P. H. (1985) *Annu. Rev. Biophys. Biophys. Chem. 14*, 131−160.
6. Northrup, S. H., Curvin M. S., Allison, S. A., and McCammon, J. A. (1986) *J. Chem. Phys. 84*, 2196−2203.
7. Northrup, S. H. (1988) *J. Phys. Chem. 92*, 5847−5850.
8. Zwanzig, R. (1990) *Proc. Natl. Acad. Sci. U.S.A. 87*, 5856−5857.
9. Wang, D., Gou S., and Axelrod, D. (1992) *Biophys. Chem. 43*, 117−137.
10. Axelrod, D., and Wang, M. D. (1994) *Biophys. J. 66*, 588−600.
11. Goldstein, B., and Dembo, M. (1995) *Biophys. J. 68*, 1222−1230.
12. Balgi, G., Leckband, D. E., and Nitsche J. M. (1995) *Biophys. J. 68*, 2251−2260.
13. Model, M. A., and Omann, G. M. (1995) *Biophys. J. 69*, 1712−1720.
14. Forsten, K. E., and Lauffenburger, D. A. (1994) *J. Comput. Biol. 1*, 15−23.
15. Lauffenburger, D. A., Forsten, K. E., Will, B., and Wiley, H. S. (1995) *Ann. Biomed. Eng. 23*, 208−215.
16. Agmon, N., and Edelstein, A. L. (1997) *Biophys. J. 72*, 1582−1594.
17. Lagerholm, B. C., and Thompson, N. L. (1998) *Biophys. J. 74*, 1215−1228.
18. Thompson, N. L., Burghardt, T. P., and Axelrod, D. (1981) *Biophys. J. 33*, 435−454.
19. Huang, Z., and Thompson, N. L. (1996) *Biophys. J. 70*, 2001−2007.
20. Pisarchick, M. L., Gesty, D., and Thompson, N. L. (1992) *Biophys. J. 63*, 215−223.
21. Pisarchick, M. L., and Thompson, N. L. (1990) *Biophys. J. 58*, 1238−1249.
22. Schweitzer-Stenner, R., Licht, A., and Pecht, I. (1992) *Biophys. J. 63*, 551−562.
23. Timbs, M. M., and Thompson, N. L. (1990) *Biophys. J. 58*, 413−428.
24. Pearce, K. H., Hiskey, R. G., and Thompson, N. L. (1992) *Biochemistry 31*, 5983−5995.

25. Poglitsch, C. L., Summner, M. T., and Thompson, N. L. (1991) *Biochemistry 30*, 6662−6671.
26. Hsieh, H. V., Poglitsch, C. L., and Thompson, N. L. (1992) *Biochemistry 31*, 11562−11566.
27. Gesty-Palmer, D. G., and Thompson, N. L. (1997) *J. Mol. Recognit. 10*, 63−72.
28. Huang, Z., Pearce, K. H., and Thompson, N. L. (1994) *Biophys. J. 67*, 1754−1766.
29. Hsieh, H. V., and Thompson, N. L. (1995) *Biochemistry 34*, 12481−12488.
30. Wright, L. L., Palmer, A. G., and Thompson, N. L. (1988) *Biophys. J. 54*, 463−470.
31. Timbs, M. M., Poglitsch, C. L., Pisarchick, M. L., Sumner, M. T., and Thompson, N. L. (1991) *Biochim. Biophys. Acta 1064*, 219−228.
32. Huang, Z., Pearce, K. H., and Thompson, N. L. (1992) *Biochim. Biophys. Acta 1112*, 259−265.
33. Pearce, K. H., Hof, M., Lentz, B. R., and Thompson, N. L. (1993) *J. Biol. Chem. 268*, 22984−22991.
34. Sheets, E. D., Chen, L., and Thompson, N. L. (1997) *Mol. Immunol. 34*, 519−526.
35. Poon, J., Bailey, M., Winzor, D. J., Davidson, B. E., and Sawyer, W. H. (1997) *Biophys. J. 73*, 3257−3264.
36. Weast, R. C., Ed. (1983) *Handbook of Chemistry and Physics*, 64th ed., p D-236, CRC Press, Boca Raton.
37. Thompson, N. L., Pearce, K. H., and Hsieh, H. V. (1993) *Eur. Biophys. J. 22*, 367−378.
38. Hellen, E. H., and Axelrod, D. (1991) *J. Fluorescence 1*, 113−128.
39. Erickson, J. W., Posner, R. G., Goldstein, B., Holowka, D., and Baird, B. (1991) *Biochemistry 30*, 2357−2363.
40. Ortega, E., Schweitzer-Sterner, R., and Pecht, I. (1991) *Biochemistry 30*, 3473−3483.
41. Posner, R. G., Lee, B., Conrad, D. H., Holowka, D., Baird, B., and Goldstein, B. (1992) *Biochemistry 31*, 5350−5356.
42. Müller, B., Zerwes, H.-G., Tangemann, K., Peter, J., and Engel, J. (1993) *J. Biol. Chem. 268*, 6800−6808.
43. Zhou, M., Felder, S., Rubinstein, M., Hurwitz, D. R., Ullrich, A., Lax, I., and Schlessinger, J. (1993) *Biochemistry 32*, 8193−8198.
44. Priestley, T., and Kemp, J. A. (1993) *Mol. Pharmacol. 44*, 1252−1257.
45. Berger, W., Prinz, H., Striessnig, J., Kang, H. C., Haugland, R., and Glossman, H. (1994) Biochemistry *33*, 11875−11883.
46. Roussiau, D. L., Staros, J. V., and Beechem, J. M., (1995) *Biochemistry 34*, 14508−14518.
47. Dunn, S. M., and Raftery, M. A. (1997) *Biochemistry 36*, 3846−3853.
48. Dunn, S. M., and Raftery, M. A. (1997) *Biochemistry 36*, 3854−3863.
49. Cowley, D. J., and Schulze, A. J. (1997) *J. Peptide Res. 49*, 444−454.
50. Hsieh, H. V., and Thompson, N. L. (1994) *Biophys. J. 66:* 898−911.
51. Thompson, N. L. (1999) unpublished results.

BI9917434